Dual-function thermoelastic cloak based on coordinate transformation theory

Yu-Ze Tan, Yan-Feng Wang, Gan-Hun Juang, Vincent Laude, Yue - Sheng Wang

Dual-function thermoelastic cloak based on coordinate transformation theory

Yu-Ze Tian,[1] Yan-Feng Wang,[1,*] Gan-Yun Huang,[1,†] Vincent Laude,[2] and Yue-Sheng Wang[1,3]

[1]*School of Mechanical Engineering, Tianjin University, 300350 Tianjin, China*
[2]*Institut FEMTO-ST, Univ. Bourgogne Franche-Comté, CNRS, Besançon, France*
[3]*Institute of Engineering Mechanics, Beijing Jiaotong University, Beijing 100044, China*

In past years, various cloaks have attracted the attention of many scientists but they usually remain confined to a single function. Cloaks combining multiple functions, however, are desirable. In this paper, we design thermoelastic cloaks with dual functionality by the coordinate transformation technique. The transformation of the thermoelastic wave equations for cloaking and explicit expressions for the required material parameters are established. Symmetrization of the elastic tensor is applied using Norris' gauge matrix to emphasize the feasibility of the designs. Two different operating conditions, transient elastic wave propagation and steady heat transfer, are adopted in numerical calculations for the designed cloaks. It is shown that, on one hand, from the perspective of observer, whether the cloak is symmetrized or not, its external response is identical and invisibility is reliable. On the other hand, it is destined that the symmetrization of the cloak would be accompanied by the increase of internal displacement, which may need to be paid attention to in the actual design. In addition, the temperature effects of both cloaks are consistent. The work in this paper may pave a way toward the realization of thermoelastic cloaks, thus broadening the research scope for metamaterials.

Keywords: Cloak; Thermoelasticity; Coordinate transformation; Metamaterials

I. INTRODUCTION

Since the concept of metamaterials was proposed, a large number of devices with abnormal properties have been designed[1]. As a popular application, the invisibility of objects has been widely discussed in different physical fields. Theories including wavefront regulation based on the generalized Snell's law[2] and active cloaks based on scattering extinction[3,4] have been widely reported. Among them, the transformation cloak has achieved wide recognition due to its flexibility and adaptability to various conditions. This type of cloak is brought out by expressing coordinate transformation invariance. Owing to the simultaneous achievement of invariance in different governing equations, objects may be made simultaneously invisible to multiphysical incident fields.

Transformation invariance was first found by Greenleaf through analysis of Maxwell's equations[5]. Building on this idea, Pendry et al.[6] and Leonhardt[7] both proposed an electromagnetic transformation cloak. A protected vacuum space would be created in the surrounding electromagnetic field, where internal objects could not be perceived externally and thus would remain hidden. Using the analogy between transverse-electric electromagnetic waves and acoustic waves in inviscid fluids, a 2D acoustic cloak was further designed by Cummer[8]. After that, Chen et al.[9] extended the result to the 3D case and a series solution for acoustic waves was given. Considering the symmetry of the biharmonic equation, a layered transformation cloak for thin plates was designed by Farhat et al.[10] with the help of effective medium theory. For a rigorous physical interpretation, Zareei et al.[11] discussed the correlation between the transformed flexural wave equation and the anisotropic plate model. Recently, Golgoon et al.[12] established a compatibility equation giving a comprehensive explanation of bending wave invisibility. On the experimental side, cloaks for electromagnetic waves[13], acoustic waves[14] and bending waves have been successfully demonstrated[15]. These results suggest a wider application of effective media theory. Based on transformation theory, cloaks have been extensively developed as well for heat flows[16], diffusion[17], water waves[18], and matter waves[19].

A difficulty is that transformation theory is not directly applicable to the Lamé-Navier equations describing elastic waves in general. The coupling of longitudinal and transverse waves makes the manipulation even more difficult. Milton et al.[20] provided an improvement for the coordinate transformation of the elastodynamic equation. The transformed elastic constitutive relations are highly consistent with the Willis equations proposed in 1981[21]. Acknowledging this fact, the designed cloak is known as a Willis-cloak. Discarding the symmetry of the elastic tensor, the transformation was further simplified by Brun et al.[22]. Nassar et al.[23] gave a solution to asymmetric constitutive relation with degenerate polar lattice. Then, based on microcontinuum theory, a static cloak has been successfully demonstrated experimentally with Cosserat materials by Xu et al[24]. Subsequently, Norris et al.[25] summarized these two types of cloaks and established a common framework. Interestingly, the above designs can be simplified if mixed modes can be separated. The proposal of pentamode metamaterials made this concept possible[26] and also provided a new pathway for the design of acoustic metasurfaces[27–29].

Since different physical fields are often associated in practice, cloaks with a single function may not provide the expected invisibility. For example, electricity and heat flows, and traveling stresses always coexist in computing devices. Temperature rise and unevenly distributed stress on the substrate are often the main reasons of damage. In the field of high-speed PCBs[30]

or chips[31], heat concentration[32,33] and the excitation of elastic waves[34,35] have attracted much attention. Syvret et al.[36] analyzed the possible breaking of thermal invisibility caused by coupling effect, illustrating the shortcomings of existing single function cloaks in a coupled field. Li et al.[37] provided a design for a dual-function transformation cloak with simultaneous heat flow and electric field regulation. This design was further expanded by Ma et al.[38] and by Stedman et al.[39]. The physical coupling effect, however, was still not considered. In the case of thermo-mechanical coupling, an elastostatic cloak under thermal gradients was designed by Alvarez et al.[40]. It can ensure the independent response of the background and the central hole. However, the cloak protection and the invisibility in the temperature field are not achieved. The design of dual-function thermoelastic cloaks including physical coupling effects thus still needs further exploration.

In this paper, we develop transformation theory under the frame of thermoelasticity. The transformed thermoelastic equations, based on Biot's thermoelasticity theory[41], are derived. Symmetrization of the transformed elastic tensor by application of a gauge matrix and the correct setting of boundary conditions is discussed. Both transformed thermoelastic equations are verified by numerical evaluation of the resulting cloaks. Their invisibility and isolation capabilities are compared. It is expected that this work can lay a theoretical foundation for transformation thermoelasticity.

II. TRANSFORMATION THEORY

The original space and the transformed space are denoted by Π and π, respectively. Particles in corresponding spaces are described by vectors X_I and x_i, between which a point-wise mapping $\mathcal{F}$ is determined. The transformation matrix is defined as $F_{iI} = \partial x_i/\partial X_I$. The uppercase and lowercase subscript correspond to the factors in two spaces respectively. Furthermore, Norris' gauge matrix A_{ij}[25] is introduced:

$$U_I = A_{iI}U_i^{'} \tag{1}$$

where U_I and $U_i^{'}$ correspond to the displacement vector fields in spaces Π and π, respectively. The summation convention on repeated subscripts is assumed.

A. Transformation thermoelasticity theory

In any subspaces $\Omega \subseteq \Pi$ the thermoelastic dynamical equations in the absence of source read:

$$\left(C_{IJKL}U_{L,K} + \beta_{IJ}\Delta T\right)_{,J} = \rho\ddot{U}_J, \tag{2}$$

$$\left(\kappa_{JL}T_{,L}\right)_{,J} = C_v\dot{T} + T_0\beta_{KL}\dot{U}_{L,K}, \tag{3}$$

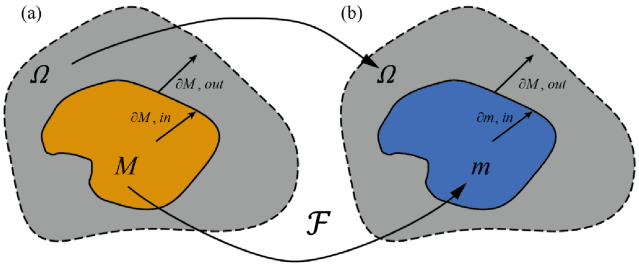

FIG. 1: Spatial configuration (a) before and (b) after coordinate transformation.

where C_{IJKL} is a fourth-order elasticity tensor satisfying the full symmetry:

$$C_{IJKL} = C_{JIKL} = C_{IJLK}, \quad C_{IJKL} = C_{KLIJ}. \tag{4}$$

ρ is the isotropic scalar mass density and C_v is the volumetric heat scalar capacity. β_{IJ} and κ_{KL} are the second-order thermal expansion tensor and thermal conductivity tensor, respectively. Anisotropy of these two tensors is allowed and their symmetry is generally guaranteed.

For simplicity, the boundary $\partial\Omega$ is set to satisfy the zero-flux condition for both physical fields:

$$n_I\left(C_{IJKL}U_{L,K} + \beta_{IJ}\Delta T\right)\mathrm{d}S|_{\partial\Omega} = 0, \tag{5}$$

$$n_J\left(\kappa_{JL}T_{,L}\right)\mathrm{d}S|_{\partial\Omega} = 0. \tag{6}$$

The physical interpretations of these conditions are traction-free and insulating boundary, respectively. These boundary conditions actually have no effect on the subsequent conclusions. We further define the stress tensor by $s_{IJ} = C_{IJKL}U_{L,K} + \beta_{IJ}\Delta T$ and the heat flux vector by $q_J = \kappa_{JL}T_{,L}$. The flux conservation relation on the boundary of an arbitrary subdomain $M \subseteq \Omega$ expresses as:

$$n_I s_{IJ}\mathrm{d}S|_{\partial M,\mathrm{in}} = n_I s_{IJ}\mathrm{d}S|_{\partial M,\mathrm{out}}\,, \tag{7}$$

$$n_J q_J\mathrm{d}S|_{\partial M,\mathrm{in}} = n_J q_J\mathrm{d}S|_{\partial M,\mathrm{out}}\,, \tag{8}$$

where the subscripts in and out are used to distinguish the inside and the outside of the boundary, as shown in Fig. 1(a).

A subdomain $m \subseteq \pi$ can be obtained by application of the mapping $m = \mathcal{F}(M)$. In general, the spatial topology of m is only determined by the mapping $\mathcal{F} : M \to m$. In this paper, its outer boundary is set to be attached to the outside of ∂M as shown in Fig. 1(b). Such a configuration ensures that the background field is not affected by the coordinate transform.

First, the continuity on the boundary ∂m needs to be guaranteed. Using the chain rule and Nanson's formula on Eqs. (7) and (8), the flux relationship under the coordinate transformation should be set as:

$$n_i' J^{-1}F_{iI}\left(C_{IJKL}U_{L,K}F_{kK} + \beta_{IJ}\Delta T\right)\mathrm{d}S\big|_{\partial m,\mathrm{in}} = n_I s_{IJ}\mathrm{d}S|_{\partial M,\mathrm{out}}\,, \tag{9}$$

$$n'_j J^{-1} F_{jJ} \left(\kappa_{JL} T_{,l} F_{lL}\right) \mathrm{d}S\big|_{\partial m,\mathrm{in}} = n_J q_J \mathrm{d}S|_{\partial M,\mathrm{out}}\,, \tag{10}$$

where $J \triangleq \det(F)$ is the Jacobian determinant of matrix F. Considering the transformed parameters:

$$C'_{iJkL} = J^{-1} F_{iI} F_{kK} C_{IJKL}, \tag{11}$$
$$\beta'_{iJ} = J^{-1} F_{iI} \beta_{IJ}, \tag{12}$$
$$\kappa'_{jl} = J^{-1} F_{jJ} F_{lL} \kappa_{JL}, \tag{13}$$
$$\rho' = J^{-1}\rho, \tag{14}$$
$$C'_v = J^{-1} C_v, \tag{15}$$

and transformed variables:

$$U'_i = U_i, \tag{16}$$
$$T' = T, \tag{17}$$

the flux relationship Eqs. (9) and(10) can be expressed as:

$$n'_i \left(C'_{iJkL} U'_{L,k} + \beta'_{iJ}\Delta T'\right) \mathrm{d}S\big|_{\partial m,\mathrm{in}} = n_I s_{IJ} \mathrm{d}S|_{\partial M,\mathrm{out}}\,, \tag{18}$$

$$n'_j \left(\kappa'_{jl} T'_{,l}\right) \mathrm{d}S\big|_{\partial m,\mathrm{in}} = n_J q_J \mathrm{d}S|_{\partial M,\mathrm{out}}\,, \tag{19}$$

while the governing equation in m under the transformed coordinate can be also obtained:

$$\left(C'_{iJkL} U'_{L,k} + \beta'_{iJ}\Delta T'\right)_{,i} = \rho' \ddot{U}'_J, \tag{20}$$
$$\left(\kappa'_{jl} T'_{,l}\right)_{,j} = C'_v \dot{T}' + T_0 \beta'_{kl} \dot{U}'_{L,k}. \tag{21}$$

The transformed boundary conditions Eqs. (18) and (19) can be noted to have the same forms as Eqs. (7) and (8) while the transformed governing equations (20) and (21) have the same forms with Eqs. (2) and (3), too. This similarity makes it possible to give an interpret physically each term in the transformed equations. In particular, the transformed thermoelastic constitutive relation reads:

$$\sigma'_{iJ} = C'_{iJkL} U'_{L,k} + \beta'_{iJ}\Delta T'. \tag{22}$$

If matrix F is not symmetric, then the asymmetry of the elastic tensor and of the thermal stress tensor results from the absence of minor symmetries:

$$C'_{iJkL} \neq C'_{JikL}, \quad C'_{iJkL} \neq C'_{iJLk}, \quad \beta'_{iJ} \neq \beta'_{iJ}. \tag{23}$$

To give an explicit physical interpretation, we define:

$$C'^{E}_{iJkL} = \frac{1}{2}\left(C'_{iJkL} + C'_{iJLk}\right), \tag{24}$$
$$D'^{E}_{iJkL} = \frac{1}{2}\left(C'_{iJkL} - C'_{iJLk}\right), \tag{25}$$
$$\omega'_{kL} = \frac{1}{2}\left(\frac{\partial U'_k}{\partial x'_L} - \frac{\partial U'_L}{\partial x'_k}\right), \tag{26}$$
$$\beta'_{iJ}\Delta T' = C'^{E}_{iJkL}\alpha'^{\varepsilon}_{kL}\Delta T' + D'^{E}_{iJkL}\alpha'^{\omega}_{kL}\Delta T'. \tag{27}$$

Furthermore Eq.(22) can be written:

$$\sigma'_{iJ} = C'^{E}_{iJkL}\left(\varepsilon'^{E}_{kL} + \alpha'^{\varepsilon}_{kL}\Delta T'\right) + D'^{E}_{iJkL}\left(\omega'^{E}_{kL} + \alpha'^{\omega}_{kL}\Delta T'\right). \tag{28}$$

ω'^{E}_{kL} is the antisymmetric rotation tensor. The two thermal related tensors $\alpha'^{\varepsilon}_{kL}$ and α'^{ω}_{kL} are the strain tensor and the rotation tensor per unit temperature, respectively. The former is obviously consistent with the linear thermal expansion tensor, the anisotropy of which is thus allowed, while the latter is a case covered in[42]. In the case that the stress σ'_{iJ} is asymmetric, the couple stress should be introduced:

$$m'_{iJ} = B'^{E}_{iJkL}\left(\varepsilon'^{E}_{kL} + \alpha'^{\varepsilon}_{kL}\Delta T'\right) + A'^{E}_{iJkL}\left(\omega^{E}_{kL} + \alpha'^{\omega}_{kL}\Delta T'\right), \tag{29}$$

where $B'^{E}_{iJkL} = D'^{E}_{kLJi}$. The constitutive relation given by Eqs. (28) and (29) is known as micropolar theory[43]. One can program these material parameters by artificially designing chiral non-centrosymmetric unit cells[44].

Eqs. (20) and (21) have similarities with Eqs. (68) and (69) given in Ref. [36]. This does not imply the commonality of coordinate transformation theory and incremental theory, however, as both theories have obvious different physical meanings. Transformation theory is built upon the mapping between different spaces Π and π from which one obtains the material parameter distribution that is required to achieve a desired function. Incremental theory builds a transformation between two different reference configurations of the same physical body, with the aim of solving problems in a unified form.

By adjusting the mapping $\mathcal{F}$, different material parameter distributions can be obtained[45]. The subdomain m would be designed as a wave-steering device with different functions, such as a rotator, a lens or an invisibility cloak. The invisibility cloak may be considered a special case as one or more holes need to be introduced in the domain represented in Fig. 1(b). Such changes in topology lead to singularities, inevitably.

When thermoelastic coupling is negligible, the above configurations will degenerate into a decoupled Cosserat-type transformation elastic cloak and a decoupled transformation heat cloak:

$$\left(C'_{iJkL} U'_{L,k}\right)_{,i} = \rho' \ddot{U}'_J, \qquad \text{in } m, \tag{30}$$
$$\left(\kappa'_{jl} T'_{,l}\right)_{,j} = C'_{\mathrm{v}} \dot{T}', \qquad \text{in } m, \tag{31}$$

with boundary conditions:

$$n'_i C'_{iJkL} U'_{L,k} \mathrm{d}S\big|_{\partial m,\mathrm{in}} = n_I C_{IJKL} U_{L,K} \mathrm{d}S|_{\partial M,\mathrm{out}}\,, \tag{32}$$

$$n'_j \kappa'_{jl} T'_{,l} \mathrm{d}S\big|_{\partial m,\mathrm{in}} = n_J \kappa_{JL} T_{,L} \mathrm{d}S|_{\partial M,\mathrm{out}}\,. \tag{33}$$

B. Symmetrized transformation thermoelasticity theory

The asymmetric constitutive relations defined by Eqs.(28) and (29) may be achieved by materials contain-

ing chiral structures, though its artificial design in this case is always limited by non-centrosymmetry[44]. However, there are many reports on the artificially designed arbitrary symmetric elastic constitutive relations[46–52] and thermal expansion tensors[53–55]. Thus, one may hope to seek an approach to make material tensors defining the devices symmetrical, at the same time retaining the performance of the design to a permissible level.

Technically, the remaining two capital subscripts in space Π in Eq. (20) need to be transformed into space π to ensure the symmetry of subscript pairs (i,j) and (k,l). In this section, the gauge transformation defined by Eq. (1) is introduced, similar to Milton et al[20] and Norris et al[25], to test the mechanism of this method under the transformation thermoelastic frame. We select $A_{iI} = F_{iI}$ in order to symmetrize the elastic and thermal expansion tensors, which leads to new governing equations. To distinguish notations from the previous section, $U_i^{''}$ is used here to represent the displacement after gauge transformation (the domain here is named differently m'):

$$\left[J^{-1}F_{iI}C_{IJKL}F_{kK}\left(A_{lL}U_l''\right)_{,k} + J^{-1}F_{iI}\beta_{IJ}\Delta T\right]_{,i} = J^{-1}\rho\left(A_{iJ}\ddot{U}_i''\right), \quad \text{in } m', \tag{34}$$

$$\left[J^{-1}F_{iI}\left(\kappa_{IJ}F_{jJ}T_{,j}\right)\right]_i = J^{-1}C_{\mathrm{V}}\dot{T} + J^{-1}F_{iI}\beta_{IJ}\left(A_{jJ}U_j''\right)_{,i}, \quad \text{in } m', \tag{35}$$

with boundary conditions:

$$n_i'J^{-1}F_{iI}\left(C_{IJKL}F_{kK}\left(A_{lL}U_l''\right)_{,k} + \beta_{IJ}\Delta T\right)\mathrm{d}S\Big|_{\partial m',\mathrm{in}} = n_I s_{IJ}\mathrm{d}S|_{\partial M,\mathrm{out}}, \tag{36}$$

$$n_i'J^{-1}F_{iI}\left(\kappa_{IJ}F_{jJ}T_{,j}\right)\mathrm{d}S\Big|_{\partial m',\mathrm{in}} = n_I q_I \mathrm{d}S|_{\partial M,\mathrm{out}}, \tag{37}$$

and implicit continuity conditions:

$$A_{iI}U_i''|_{\partial m',\mathrm{in}} = U_I|_{\partial M,\mathrm{out}}, \tag{38}$$

After these processes, the physical meaning of the terms in Eq.(34) is still unclear. The mass density is effectively not only anisotropic but also asymmetric. The coupling terms in Eq. (34) and Eq. (35) do not match as well. Gauge freedom can be invoked again: gauge matrix A_{iI} can be multiplied with the free index I on both sides of Eq. (34). Mathematically, it means only considering a linear combination of the system of equations, which is equivalent to the initial system of equation if A is non singular. For the same reason, boundary condition Eq. (36) is preserved. The distribution of displacement would not be changed due to the uniqueness of the solution of the wave equation:

$$A_{jJ}\left[J^{-1}F_{iI}C_{IJKL}F_{kK}\left(A_{lL}U_l''\right)_{,k} + J^{-1}F_{iI}\beta_{IJ}\Delta T\right]_{,i} = J^{-1}A_{jJ}\rho\left(A_{iJ}\ddot{U}_i''\right), \text{ in } m'. \tag{39}$$

Because the gauge matrix only rearranges the distribution of the displacement U_i inside subdomain m, the external environment is not influenced, and the same solution as in Eq. (20) can be obtained. Still, it is difficult to explain the physical meaning of the equation clearly. Using the identity:

$$\left(P_{ij}Q_{jk}\right)_{,i} = \left(P_{ij}\right)_{,i}Q_{jk} + P_{ij}\left(Q_{jk}\right)_{,i}, \tag{40}$$

Eq. (39) can be transformed into a new governing equation:

$$\left(C_{ijkl}''U_{l,k}'' + S_{ijl}''U_l'' + \beta_{ij}''\Delta T\right)_{,i} = \rho_{ij}''\ddot{U}_i'' + D_{jkl}''U_{k,l}'' + E_{jl}''U_l'' + \gamma_j''\Delta T, \quad \text{in } m', \tag{41}$$

with:

$$C_{ijkl}'' = J^{-1}F_{iI}A_{jJ}F_{kK}A_{lL}C_{IJKL}, \tag{42}$$
$$S_{ijl}'' = J^{-1}F_{iI}A_{jJ}A_{lL,K}C_{IJKL}, \tag{43}$$
$$D_{jkl}'' = J^{-1}A_{jJ,I}F_{kK}A_{lL}C_{IJKL}, \tag{44}$$
$$E_{jl}'' = J^{-1}A_{jJ,I}A_{lL,K}C_{IJKL}, \tag{45}$$
$$\rho_{ij}'' = J^{-1}A_{iI}A_{jJ}\rho, \tag{46}$$
$$\beta_{ij}'' = J^{-1}F_{iI}A_{jJ}\beta_{IJ}, \tag{47}$$
$$\gamma_j'' = J^{-1}A_{jJ,I}\beta_{IJ}. \tag{48}$$

Due to the limitation of Eq.(38) , the degradation condition needs to be introduced on the boundary:

$$A_{iI}|_{\partial m',\mathrm{in}} = I_{iI}|_{\partial m',\mathrm{in}}. \tag{49}$$

where I_{iI} is the identity matrix. Therefore a more general continuity condition can be obtained:

$$U_I''|_{\partial m',\mathrm{in}} = U_I|_{\partial M,\mathrm{out}}. \tag{50}$$

with the stress equilibrium boundary condition:

$$n_i'\left(C_{ijkl}''U_{l,k}'' + S_{ijl}''U_l'' + \beta_{ij}''\Delta T\right)\mathrm{d}S\Big|_{\partial m',\mathrm{in}} = n_I s_{Ij}\mathrm{d}S|_{\partial M,\mathrm{out}}. \tag{51}$$

Since the gauge matrix is only a local transformation of the dependent variable, the normal vector n_i' in Eq.(51) would not be changed. The adjustment from Eq.(39) to Eq.(41) does accompany the change of flux/stress relationship, but the displacement field U_i'' is not affected. One can choose an arbitrary subdomain Φ within m', on whose boundary $\partial\Phi$ the flux condition derived from Eq.(39) reads:

$$n_i'J^{-1}F_{iI}\left(C_{IJKL}F_{kK}\left(A_{lL}U_l''\right)_{,k} + \beta_{IJ}\Delta T\right)\mathrm{d}S\Big|_{\partial\Phi,\mathrm{in}} = n_i'J^{-1}F_{iI}\left(C_{IJKL}F_{kK}\left(A_{lL}U_l''\right)_{,k} + \beta_{IJ}\Delta T\right)\mathrm{d}S\Big|_{\partial\Phi,\mathrm{out}}, \tag{52}$$

while the one derived from Eq.(41) reads:

$$n_i'\left(C_{ijkl}''U_{l,k}'' + S_{ijl}''U_l'' + \beta_{ij}''\Delta T\right)\mathrm{d}S\Big|_{\partial\Phi,\mathrm{in}} = n_i'\left(C_{ijkl}''U_{l,k}'' + S_{ijl}''U_l'' + \beta_{ij}''\Delta T\right)\mathrm{d}S\Big|_{\partial\Phi,\mathrm{out}}. \tag{53}$$

Eqs.(52) and (53) are the specific expressions of Cauchy formula with different definitions of stress given by Eqs.(39) and (41), respectively. It is obvious that they are inconsistent in physical meaning. After multiplying both ends of Eq.(52) by A_{jJ}, it would be noticed that the two actually have the same constraint on U_i''. In addition, considering the degradation condition Eq.(49), Eq.(36) is equivalent to Eq.(50) on $\partial m'$. Therefore, the conclusion can be drawn that the above process would not make any differences to the performance of our target.

Then, we represent the temperature in heat-conduction equations (21) under transformed coordinates:

$$T'' = T, \tag{54}$$

with the parameters:

$$\kappa''_{jl} = J^{-1}F_{jJ}F_{lL}\kappa_{JL}, \tag{55}$$

$$C''_{\mathrm{V}} = J^{-1}C_{\mathrm{V}}, \tag{56}$$

The symmetrized transformation thermoelastic governing equations and boundary conditions are given by:

$$\begin{gathered}
\left(C''_{ijkl}U''_{l,k} + S''_{ijl}U''_{l} + \beta''_{ij}\Delta T''\right)_{,i} = \\
\rho''_{ij}\ddot{U}''_{i} + D''_{jkl}U''_{k,l} + E''_{jl}U''_{l} + \gamma''_{j}\Delta T'', \quad \text{in } m', \\
\left(\kappa''_{jl}T''_{,l}\right)_{,j} = C''_{\mathrm{V}}\dot{T}'' + \beta''_{kl}T_0\dot{U}''_{l,k} + \gamma''_{l}T_0\dot{U}''_{l}, \quad \text{in } m', \\
n'_i\left(C''_{ijkl}U''_{l,k} + S''_{ijl}U''_{l} + \beta''_{ij}\Delta T''\right)\mathrm{d}S\big|_{\partial m',\mathrm{in}} = \\
n_I S_{Ij}\mathrm{d}S\big|_{\partial M,\mathrm{out}}, \\
n'_j\left(\kappa''_{jl}T''_{,l}\right)\mathrm{d}S\big|_{\partial m',\mathrm{in}} = n_I q_I \mathrm{d}S\big|_{\partial M,\mathrm{out}}.
\end{gathered} \tag{57}$$

Interestingly, although the displacement field is changed by both gauge matrix and coordinate transformation matrix, the temperature field is only affected by the latter. Therefore, a same temperature distribution with the asymmetric transformation thermoelasticity theory would be obtained under the symmetrized one.

Similar to the previous discussion, when the thermoelastic coupling effect is negligible, the above equations will degenerate into a decoupled Willis-type transformation elastic cloak and a decoupled transformation heat cloak:

$$\left(C''_{ijkl}U''_{l,k} + S''_{ijl}U''_{l}\right)_{,i} = \rho''_{ij}\ddot{U}''_{i} + D''_{jkl}U''_{k,l} + E''_{jl}U''_{l}, \ \text{in } m', \tag{58}$$

$$\left(\kappa''_{ij}T''_{,j}\right)_{,i} = C''_{\mathrm{V}}\dot{T}'' \quad \text{in } m', \tag{59}$$

with boundary conditions:

$$\begin{gathered}
n'_i\left(C''_{ijkl}U''_{l,k} + S''_{ijl}U''_{l}\right)\mathrm{d}S\big|_{\partial m',\mathrm{in}} = \\
n_I\left(C_{IJKL}U_{L,K}\right)\mathrm{d}S\big|_{\partial M,\mathrm{out}},
\end{gathered} \tag{60}$$

$$n'_j\left(\kappa''_{jl}T''_{,l}\right)\mathrm{d}S\big|_{\partial m',\mathrm{in}} = n_J q_J \mathrm{d}S\big|_{\partial M,\mathrm{out}}. \tag{61}$$

III. SIMULATION RESULTS

In this section, both transformation thermoelasticity theories described in Sect. II.A and Sect. II.B are explored within the context of an invisibility cloak. For convenience, they are designated as asymmetric and symmetrized dual-function thermoelastic cloaks, respectively. Their performance is evaluated through numerical simulation by comparing with the cases of a uniform medium and of an unprotected hole. The partial differential equation (PDE) package of COMSOL multiphysics is used for numerical calculations in this paper. Due to the continuity condition of Eq.(49) that is introduced by the symmetrization process, the linear affine mapping that is generally considered in the literature is not applicable. Instead, a nonlinear transformation $\mathcal{F}$ is adopted. It reads in cylindrical coordinates:

$$r' = \frac{r_1}{r_2^2}r^2 + \frac{r_2 - 2r_1}{r_2}r + r_1, \quad \theta' = \theta, \quad z' = z, \quad r \in M, \tag{62}$$

with the monotonicity condition:

$$r_2 \geq 2r_1, \tag{63}$$

where r_1 and r_2 are the inner radius and outer radius of the cloak. $\mathcal{F}$ satisfies $r'(r_2) = r_2$, $r'(0) = r_1$, and $\mathrm{d}r'/\mathrm{d}r(r_2) = 1$. Matrix F reads in Cartesian coordinates:

$$F = R(\theta')\begin{bmatrix} \mathrm{d}r'/\mathrm{d}r & 0 & 0 \\ 0 & r'/r & 0 \\ 0 & 0 & 1 \end{bmatrix}R(-\theta') \tag{64}$$

where

$$r\left(r'\right) = \frac{\sqrt{\left(r_2 - 2r_1\right)^2 + 4r_1\left(r' - r_1\right)} - \left(r_2 - 2r_1\right)}{\frac{2r_1}{r_2}}. \tag{65}$$

Consequently, the region $r' < r_1$ is removed from space Ω so that anything placed there would be invisible. One should mention that for a perfect cloak, $\mathcal{F}(\mathbf{X} = \mathbf{O})$ may not represent a single point in m. However, it will inevitably lead to infinite material parameters, so we replace it with a micropore near the point $\mathbf{X} = \mathbf{O}$ which would be called as inner-diameter defect in this paper.

Copper is taken as the background medium characterized by lamé constants $\lambda = 95$ GPa and $\mu = 40$ GPa, mass density $\rho = 8960$ kg/m^3, isotropic thermal conductivity $\kappa = 397$ W/(m $\cdot$ K), volumetric heat capacity $C_{\mathrm{V}} = 3.5$ J/ $\left(\mathrm{m}^3 \cdot \mathrm{K}\right)$ and isotropic thermal expansion coefficient $\beta = 6$MPa/K.

A. Transient elastic wave

High-frequency compressional waves excited by thermal-electro-mechanical coupling are a major problem on microelectronic substrates. Energy transfers

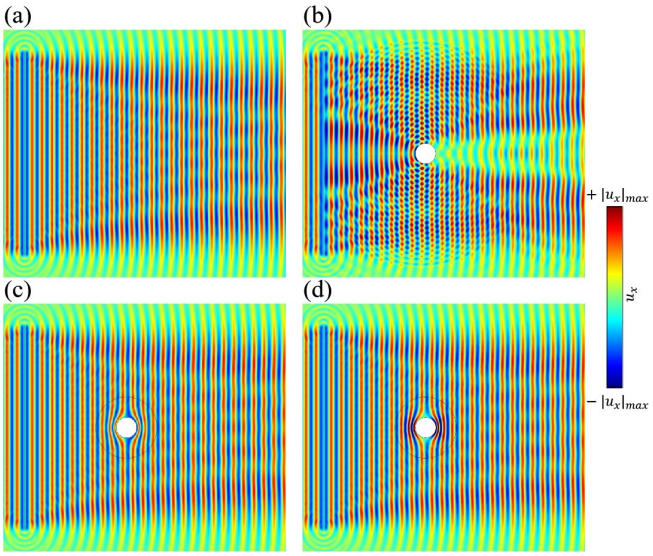

FIG. 2: Distribution of displacement u_x under the excitation of elastic waves in different systems: (a) a homogeneous isotropic medium; (b) the same medium with a traction-free hole; (c) the traction-free hole covered with the asymmetric dual-function thermoelastic cloak; (d) the traction-free hole covered with the symmetrized dual-function thermoelastic cloak.

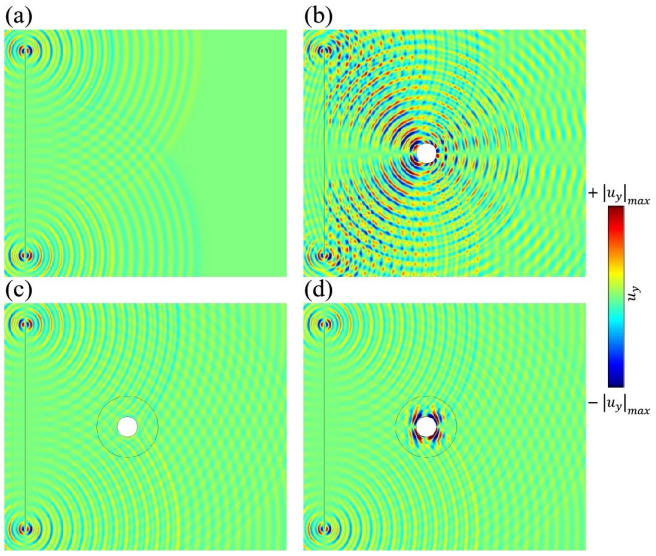

FIG. 3: Distribution of displacement u_y under the excitation of elastic waves in different systems: (a) a homogeneous isotropic medium; (b) the same medium with a traction-free hole; (c) the traction-free hole covered with the asymmetric dual-function thermoelastic cloak; (d) the traction-free hole covered with the symmetrized dual-function thermoelastic cloak.

between different components in the form of temperature (heat) and mechanical (elastic wave) fluctuations, and finally concentrates at the holes. Thermoelastic energy concentration is one of the main reasons for the reduction of the service life of components and equipments, especially under heavy computational loads. Protective cloaks possibly could reduce this phenomenon.

The numerical model in this section is set as follows. A $L = 20l_0$ long x-polarization line excitation source, located to the left of the cloak a distance $d = 10l_0$ from its center, oscillates at frequency $f_0 = 150$ kHz with an amplitude of $A_0 = 100$ μm. The wavelength of the incident longitudinal wave is $l_0 = \sqrt{\lambda + 2\mu/\rho}/f_0 = 29.4$ mm. The inner and outer radius of the cloak is set to $r_1 = l_0$ and $r_2 = 3l_0$, respectively. To ensure convergence, the maximum mesh element size is set to one twentieth of the wavelength l_0. Transient analysis is performed, since the governing equation for temperature in (3) is a diffusion equation without time-harmonic characteristics. The background boundary is set as both traction-free and thermally insulating, following Eqs. (5) and (6). The exact boundary condition has no incidence on the results as long as the background medium is chosen wide enough to avoid reflections. The inner boundary of the cloak is set as traction-free and thermally insulating as well.

The displacement along the x-direction shown in Fig. 2 is the primary physical variable under investigation. For reference, Fig. 2(a) shows the unimpeded propagation of thermoelastic waves. Due to the introduction of a hole, as shown in Fig. 2(b), forward propagation of the wave is partially blocked and scattering to the upper and lower sides occurs. Scattering is well removed after covering the hole with the asymmetric dual-function thermoelastic cloak, as shown in Fig. 2(c). The hole is effectively isolated from the background medium by the cloak and has thus little influence on the displacement field. Things are a little different when the symmetrized dual-function thermoelastic cloak covers the hole, as shown in Fig. 2(d). Consistently with the analysis of Sect. II.B, the displacement field outside the cloak region appears visually the same as in Fig. 2(c). However, the displacements inside the cloak is significantly rearranged by the gauge matrix. Since Eq. (1) does not define a norm preserving mapping, the amplitude obviously changes. This peculiarity does not affect invisibility but creates some concentration of energy around the hole.

The contrast is more prominent considering the displacement along the y direction, as shown in Fig. 3. Compared with the displacement concentration at the edge of the finite line source, the displacement caused by scattering at the hole in Fig. 3(b) is dominant. The asymmetric dual-function thermoelastic cloak shown in Fig. 3(c) ensures that the external environment is almost unaffected by the hole. The symmetrized cloak shown in Fig. 3(d) also hides the hole in the far field, but some energy concentration occurs in its interior. The difference between both cloaks may be explained from the perspective of the constitutive relations. The asymmetric cloak adopts a constitutive relationship similar to that of chiral materials, see Eqs. (28) and (29). The rotational stiffness is thus the main factor in wave manipulation. In contrast, the symmetrized cloak mainly depends on the

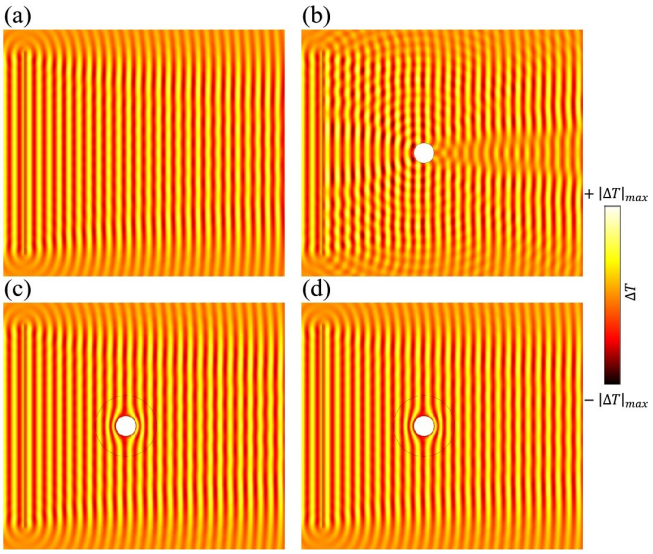

FIG. 4: Distribution of the temperature variation ΔT under the excitation of elastic waves in different systems: (a) a homogeneous isotropic medium; (b) the same medium with a traction-free hole; (c) the traction-free hole covered with the asymmetric dual-function thermoelastic cloak; (d) the traction-free hole covered with the symmetrized dual-function thermoelastic cloak.

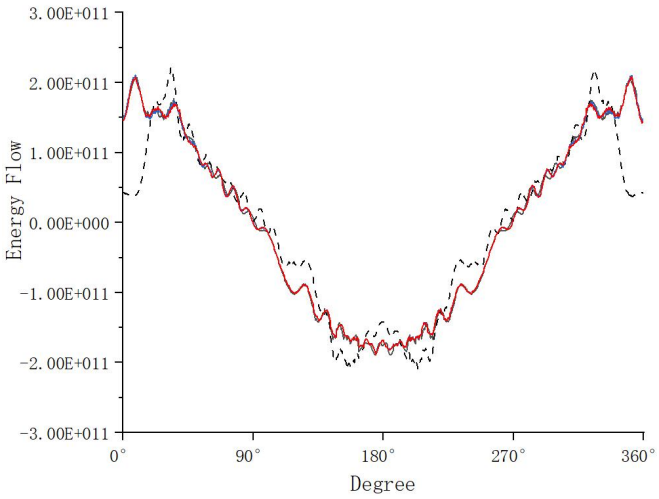

FIG. 5: Power flow at distance $r = 6l_0$ as a function of direction. Considered are the homogeneous isotropic medium (black solid curve), the traction-free hole (black dashed curve), the traction-free hole covered with an asymmetric dual-function thermoelastic cloak (blue solid curve), the traction-free hole covered with a symmetrized dual-function thermoelastic cloak (red solid curve).

unique Willis coupling terms and on the anisotropic mass of Willis materials. As a consequence, waves are redirected by means of the coupling of vibrations along different directions. The difference in the regulation mechanisms may also provide a physical interpretation to the differences in Fig. 2(c)(d). In addition, consistent invisibility of external fields in Figs. 2(c)(d) and Figs. 3(c)(d) is also observed for both regulation mechanisms. This results from the fact that Willis materials share similar characteristics with chiral materials[56], even if coupling is considered. However, for the practical application of symmetrized cloaks based on Willis materials, more attention should be paid to the dramatic increase in internal displacement fields.

Fig. 4 shows the thermal field accompanying high frequency waves, which also implies the transfer of thermal energy on the substrate. The temperature field is mainly dominated by time-dependent terms in Eq. (3), the volumetric heat capacity in Eqs. (15) and (56), and the thermal expansion tensors in Eqs. (12), (47) and (48). Fig. 4(b) shows the change in the temperature field resulting from the introduction of a hole in the uniform medium. The temperature distribution is obviously affected. Thermal concentration would lead energy to accumulate at the hole over time, which is potentially harmful to the inserts contained in it. Different from the displacement fields, both cloaks (see Fig. 4(c,d)) mask the presence of the hole and guide the heat flow smoothly around it with the same signature. This observation is consistent with the statement that the introduction of the gauge matrix does not affect the temperature field.

Furthermore, under the same design strategy, the asymmetric dual-function cloak using chiral materials and the symmetrized cloak using Willis materials always share the same thermal coupling characteristics. The symmetry process is thus not affected by coupling.

For quantitative analysis, the disturbance caused by the introduction of the hole and of the cloak must be obtained. Under thermal coupling, the scattered-field formulation may be no longer be applicable. Radiation characteristics are here described by the time-averaged power flow defined by

$$e\left(\boldsymbol{r}, t_0\right)=\frac{1}{T}\int_{t_0}^{t_0+T}-\boldsymbol{n}(\boldsymbol{r})\cdot[\boldsymbol{\sigma}(\boldsymbol{r},t)\cdot\dot{\boldsymbol{u}}(\boldsymbol{r},t)+\boldsymbol{\kappa}(\boldsymbol{r})\cdot\nabla T(\boldsymbol{r},t)]\mathrm{d}t. \tag{66}$$

This formula combines both elastic and thermal radiation. Fig. 5 shows power flow from the region $r < 6l_0$ (abbreviated as $\boldsymbol{\psi}$) as a function of direction, for different configurations. Negative $e\left(\boldsymbol{r}_0, t_0\right) < 0$ indicates that power flows into $\boldsymbol{\psi}$ at point $\boldsymbol{r}_0$, whereas positive $e\left(\boldsymbol{r}_0, t_0\right) > 0$ indicates power radiates from $\boldsymbol{\psi}$ at point $\boldsymbol{r}_0$. Since the thermoelastic wave is incident from the left, region $\boldsymbol{\psi}$ always receives power in angles in the range $[90°, 270°]$ and radiates power in other directions. The homogeneous isotropic media is considered as a reference. After introduction of the hole, scattering from its edge causes a significant change in the power flow characteristics, resulting in a low correlation of 93.15%. Changes are most prominent around 0° and in the range $[90°, 270°]$. When the hole is covered with an asymmetric cloak or a symmetrized cloak, the power flow distribution almost coincides with the reference one. The correlation is restored to 99.95% and 99.94%, respectively. Minor devia-

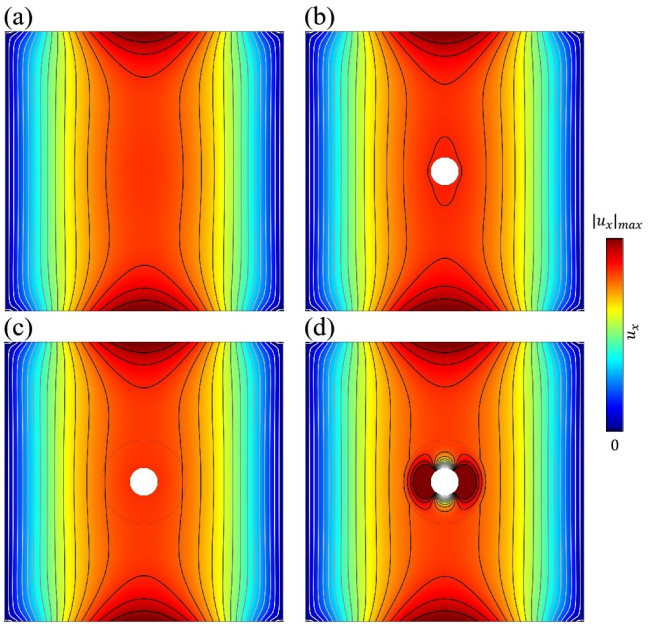

FIG. 6: Distribution of displacement u_x under heat flow for different systems: (a) a homogeneous isotropic medium; (b) the same medium with a traction-free hole; (c) the traction-free hole covered with the asymmetric dual-function thermoelastic cloak; (d) the traction-free hole covered with the symmetrized dual-function thermoelastic cloak.

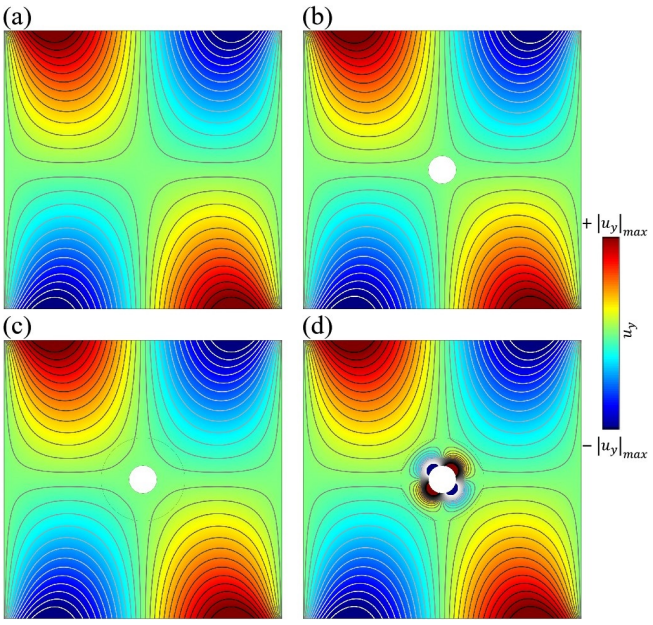

FIG. 7: Distribution of displacement u_y under heat flow for different systems: (a) a homogeneous isotropic medium; (b) the same medium with a traction-free hole; (c) the traction-free hole covered with the asymmetric dual-function thermoelastic cloak; (d) the traction-free hole covered with the symmetrized dual-function thermoelastic cloak.

tions, mainly caused by internal diameter defects, can be noticed; though they may be unavoidable they remain inconsequential. In addition, the high coincidence for both cloaks (with a correlation of 99.99%) also shows the practical equivalence of the two transformation thermoelastic theories with regards to radiation.

B. Steady heat transfer

The performance of both cloaks is now tested under the application of a temperature gradient applied between the left and right sides of the computation domain. The numerical model is set as follows. A square with length L is set as the substrate. Its center coincides with the center of the cloak. The inside and outside radiuses of the cloak are identical to Section 3.1. A temperature difference $\Delta T = 60K$ is applied between the left and the right sides of the substrate. Both upper and lower boundaries, and holes are set as traction-free and thermally insulating boundaries. Steady state analysis is adopted here.

The displacements u_x and u_y caused by the temperature difference are shown in Fig. 6 and Fig. 7. As shown in Fig. 6(a), displacements are enhanced at the free boundaries of the homogeneous substrate. After introduction of the hole, as shown in Fig. 6(b), displacements around the hole increase slightly. The asymmetric cloak shown in Fig. 6(c) counters this increase while leaving the substrate apparently unaffected by the hole. In the case of the symmetrized cloak (Fig. 6(d)), invisibility is still guaranteed. However, the Willis material used in the cloak under steady state shows obvious flexibility, which results in significant displacement variations inside the cloak. Although it has no effect on the background medium, this concentration may lead to compression of inserts placed the hole. Similar features are observed are Fig. 7. The concentration introduced by the symmetrization process is contrary to expectations and may need further improvements. In summary, on the one hand, both dual-function cloaks under heat flow provide invisibility; on the other hand, the symmetrization process may destroy the elastic isolation of the hole from the background media.

The temperature field shown in Fig. 8 is governed only by the steady-state heat conduction equation:

$$\left(\kappa_{IJ}T_{,J}\right)_{,I} = 0. \tag{67}$$

The direction of heat flow in both cloaks is determined by the transformed thermal conductivity (Eq.13) with the governing equation:

$$\left(\kappa'_{ij}T'_{,j}\right)_{,i} = 0, \tag{68}$$

which is the same as the traditional heat cloak[16]. Obviously, the temperature field is decoupled in the steady state. Therefore, relevant conclusions are consistent with the previous literature on the heat cloak.

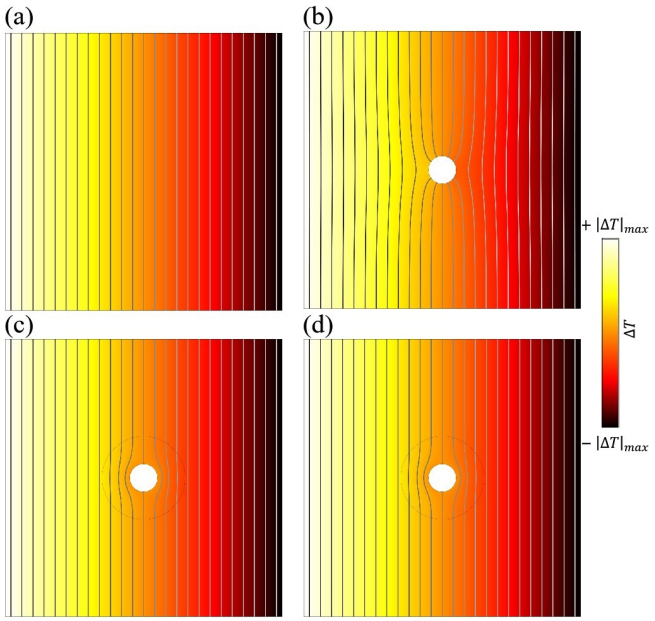

FIG. 8: Distribution of the temperature variation ΔT under heat flow for different systems: (a) a homogeneous isotropic medium; (b) the same medium with a traction-free hole; (c) the traction-free hole covered with the asymmetric dual-function thermoelastic cloak; (d) the traction-free hole covered with the symmetrized dual-function thermoelastic cloak.

IV. DISCUSSION AND CONCLUSION

In this paper, transformation theory has been extended to the framework of thermoelasticity. The governing equations for transformation thermoelasticy are derived. Two transformation strategies, involving either asymmetric or symmetrized elastic tensors, are given. The influence of the symmetrization process on boundary conditions is included. Degenerate conditions are proposed to ensure its feasibility. Numerical simulations are conducted to analyze the regulation mechanisms of both theories within the context of a dual-function thermoelastic invisibility cloak designed from a nonlinear coordinate transformation. Two operation conditions are considered.

Under transient elastic wave excitation, both cloaks ensure invisibility and isolation of the hole from the outside field. The identity of the two transformation thermoelasticity theories has been verified. Very similar temperature fields are obtained for both theories under the same design strategy. Mathematical and physical interpretations are given for the differences in the displacement fields resulting from the symmetrization process. A time-averaged power flow is proposed to verify quantitatively the performance of the cloaks.

Under steady heat transfer, it is still found that invisibility is maintained for both displacement and temperature fields. However, the Willis material used in the symmetrized cloak shows obvious softness in the steady state, with large displacements around the holes. This characteristic may result in compression of inserts in the hole.

Our work attempts to advance transformation theory to the thermoelastic framework. It is still worth noting that the asymmetric thermal expansion tensor and the newly introduced physical quantities resulting from symmetrization still need further exploration. From the perspective of transformation thermoelasticity, the cloak concept appears to be valuable, owing to the fact that the terms of displacement coupling and displacement gradient coupling are in similar positions with the temperature-dependent terms in Eq. (54). Further work to be carried out include finding an approximate solution for the structure of the cloak with the help of effective medium theory, and performing experimental demonstrations.

V. ACKNOWLEDGMENTS

The authors acknowledge financial support by the National Natural Science Foundation of China (12122207 and 12021002). Y.F.W. acknowledges support by the Natural Science Foundation of Tianjin, China (20JCQNJC01030). V.L. acknowledges financial support by the EIPHI Graduate School (ANR-17-EURE-0002).

* Electronic address: wangyanfeng@tju.edu.cn
† Electronic address: gyhuang@tju.edu.cn

[1] Y.-F. Wang, Y.-Z. Wang, B. Wu, W. Chen, and Y.-S. Wang, Applied Mechanics Reviews **72**, 040801 (2020).
[2] X. Ni, Z. J. Wong, M. Mrejen, Y. Wang, and X. Zhang, Science **349**, 1310 (2015).
[3] Y. R. Padooru, A. B. Yakovlev, P.-Y. Chen, and A. Alu, Journal of Applied Physics **112**, 034907 (2012).
[4] D. Rainwater, A. Kerkhoff, K. Melin, J. Soric, G. Moreno, and A. Alù, New Journal of Physics **14**, 013054 (2012).
[5] A. Greenleaf, M. Lassas, and G. Uhlmann, arXiv preprint math/0302258 (2003).
[6] J. B. Pendry, D. Schurig, and D. R. Smith, science **312**, 1780 (2006).
[7] U. Leonhardt, science **312**, 1777 (2006).
[8] S. A. Cummer and D. Schurig, New journal of physics **9**, 45 (2007).
[9] H. Chen and C. Chan, Applied physics letters **91**, 183518 (2007).
[10] M. Farhat, S. Guenneau, S. Enoch, and A. B. Movchan, Physical Review B **79**, 033102 (2009).
[11] A. Zareei and M.-R. Alam, Physical Review E **95**, 063002 (2017).
[12] A. Golgoon and A. Yavari, Journal of Nonlinear Science **31**, 1 (2021).
[13] D. Schurig, J. J. Mock, B. Justice, S. A. Cummer, J. B.

Pendry, A. F. Starr, and D. R. Smith, Science **314**, 977 (2006).
[14] B.-I. Popa, L. Zigoneanu, and S. A. Cummer, Physical review letters **106**, 253901 (2011).
[15] A. Darabi, A. Zareei, M.-R. Alam, and M. J. Leamy, Physical review letters **121**, 174301 (2018).
[16] C. Fan, Y. Gao, and J. Huang, Applied Physics Letters **92**, 251907 (2008).
[17] S. Guenneau and T. Puvirajesinghe, Journal of The Royal Society Interface **10**, 20130106 (2013).
[18] M. Farhat, S. Enoch, S. Guenneau, and A. Movchan, Physical review letters **101**, 134501 (2008).
[19] S. Zhang, D. A. Genov, C. Sun, and X. Zhang, Physical Review Letters **100**, 123002 (2008).
[20] G. W. Milton, M. Briane, and J. R. Willis, New Journal of Physics **8**, 248 (2006).
[21] J. R. Willis, Wave Motion **3**, 1 (1981).
[22] M. Brun, S. Guenneau, and A. B. Movchan, Applied physics letters **94**, 061903 (2009).
[23] H. Nassar, Y. Chen, and G. Huang, Proceedings of the Royal Society A **474**, 20180523 (2018).
[24] X. Xu, C. Wang, W. Shou, Z. Du, Y. Chen, B. Li, W. Matusik, N. Hussein, and G. Huang, Physical review letters **124**, 114301 (2020).
[25] A. N. Norris and A. L. Shuvalov, Wave Motion **48**, 525 (2011).
[26] A. N. Norris, Proceedings of the Royal Society A: Mathematical, Physical and Engineering Sciences **464**, 2411 (2008).
[27] L. He, L. Cai, and X. Chen, Journal of Applied Mathematics and Physics **9**, 1829 (2021).
[28] Y. Gu, H. Long, Y. Cheng, M. Deng, and X. Liu, Physical Review Applied **16**, 014021 (2021).
[29] Z. Sun, Y. Shi, X. Sun, H. Jia, Z. Jin, K. Deng, and J. Yang, Journal of Physics D: Applied Physics **54**, 205303 (2021).
[30] S.-J. Joo, B. Park, D.-H. Kim, D.-O. Kwak, J. Park, and H.-S. Kim, Journal of Micromechanics and Microengineering **26**, 045006 (2016).
[31] M. Nagaraj and C. S. Suh, IEEE Transactions on Device and Materials Reliability **5**, 224 (2005).
[32] S. Arakelyan, H. Lee, Y. Jeong, A. Babajanyan, B. Friedman, and K. Lee, Case studies in thermal engineering **10**, 407 (2017).
[33] H. Lee, S. Arakelyan, B. Friedman, and K. Lee, Scientific reports **6**, 1 (2016).
[34] X. Qi and C. S. Suh, International journal of heat and mass transfer **53**, 41 (2010).
[35] X. Qi and C. S. Suh, International journal of heat and mass transfer **53**, 744 (2010).
[36] F. Syvret and D. Al-Attar, arXiv preprint arXiv:1903.06664 (2019).
[37] J. Li, Y. Gao, and J. Huang, Journal of Applied Physics **108**, 074504 (2010).
[38] Y. Ma, Y. Liu, M. Raza, Y. Wang, and S. He, Physical review letters **113**, 205501 (2014).
[39] T. Stedman and L. M. Woods, Scientific reports **7**, 1 (2017).
[40] J. C. Á. Hostos, V. D. Fachinotti, and I. Peralta, Scientific reports **9**, 1 (2019).
[41] M. A. Biot, Journal of applied physics **27**, 240 (1956).
[42] C. S. Ha, E. Hestekin, J. Li, M. E. Plesha, and R. S. Lakes, physica status solidi (b) **252**, 1431 (2015).
[43] A. C. Eringen, *Microcontinuum field theories: I. Foundations and solids* (Springer Science & Business Media, 2012).
[44] I. Fernandez-Corbaton, C. Rockstuhl, P. Ziemke, P. Gumbsch, A. Albiez, R. Schwaiger, T. Frenzel, M. Kadic, and M. Wegener, Advanced Materials **31**, 1807742 (2019).
[45] H. Chen and C. T. Chan, Journal of Physics D: Applied Physics **43**, 113001 (2010).
[46] B. Ling, K. Wei, Z. Qu, and D. Fang, International Journal of Mechanical Sciences **195**, 106220 (2021).
[47] B. Ling, K. Wei, Z. Wang, X. Yang, Z. Qu, and D. Fang, International Journal of Mechanical Sciences **173**, 105466 (2020).
[48] X. Chen, N. Laforge, Q. Ji, H. Tan, J. Liang, G. Ulliac, J. Moughames, S. Adrar, V. Laude, and M. Kadic, Comptes Rendus. Physique **21**, 751 (2020).
[49] G. W. Milton and A. V. Cherkaev (1995).
[50] G. Yi and B. D. Youn, Structural and Multidisciplinary Optimization **54**, 1315 (2016).
[51] C. B. Dilgen, S. B. Dilgen, N. Aage, and J. S. Jensen, Structural and Multidisciplinary Optimization **60**, 779 (2019).
[52] W. Li, F. Meng, Y. Chen, Y. f. Li, and X. Huang, Advanced Theory and Simulations **2**, 1900017 (2019).
[53] X. Ni, X. Guo, J. Li, Y. Huang, Y. Zhang, and J. A. Rogers, Advanced Materials **31**, 1905405 (2019).
[54] K. Wei, X. Xiao, J. Chen, Y. Wu, M. Li, and Z. Wang, Materials & design **198**, 109343 (2021).
[55] X. Guo, X. Ni, J. Li, H. Zhang, F. Zhang, H. Yu, J. Wu, Y. Bai, H. Lei, Y. Huang, et al., Advanced Materials **33**, 2004919 (2021).
[56] M. Kadic, A. Diatta, T. Frenzel, S. Guenneau, and M. Wegener, Physical Review B **99**, 214101 (2019).